

Document downloaded from the institutional repository of the University of Alcalá: <http://ebuah.uah.es/dspace/>

This is a preprint version of the following published document:

Regadío, A., Sánchez-Prieto, S., Prieto, M. & Tabero, J., 2014, "Implementation of a real-time adaptative digital shaping for nuclear spectroscopy", Nuclear Instruments and Methods in Physics Research Section A, vol. 735, pp. 297-303

Available at <https://doi.org/10.1016/j.nima.2013.09.063>

© 2014 Elsevier

(Article begins on next page)



This work is licensed under a

Creative Commons Attribution-NonCommercial-NoDerivatives
4.0 International License.

Implementation of a real-time adaptive digital shaping for nuclear spectroscopy

Alberto Regadío^{a,b,*}, Sebastián Sánchez-Prieto^a, Manuel Prieto^a, Jesús Tabero^b

^a*Department of Computer Engineering, Space Research Group, Universidad de Alcalá, 28805 Alcalá de Henares, Spain*

^b*Electronic Technology Area, Instituto Nacional de Técnica Aeroespacial, 28850 Torrejón de Ardoz, Spain*

Abstract

This paper presents the structure, design and implementation of a new adaptive digital shaper for processing the pulses generated in nuclear particle detectors. The proposed adaptive algorithm has the capacity to automatically adjust the coefficients for shaping an input signal with a desired profile in real-time. Typical shapers such as triangular, trapezoidal or cusp-like ones can be generated, but more exotic unipolar shaping could also be performed. A practical prototype was designed, implemented and tested in a Field Programmable Gate Array (FPGA). Particular attention was paid to the amount of internal FPGA resources required and to the sampling rate, making the design as simple as possible in order to minimize power consumption. Lastly, its performance and capabilities were measured using simulations and a real benchmark.

Keywords: Spectroscopy, Shaping, Adaptive, Signal processing, FPGA, Nuclear detectors

1. Introduction

1 Nuclear spectroscopy is the term used to describe the electronic systems employed to study elemental
2 particles and nuclear physics. These techniques have become extensively used in many fields, such as radi-
3 ation detection or space particle telescopes. Typical elements of these devices include high-speed detectors
4 to measure rates and energy, preamplifiers, shapers, discriminators, counters and pulse height analyzers
5 [1]. From the point of view of signal transformation, the weak and fast pulse provided by the detectors is
6 amplified and filtered to optimize detection. This process has traditionally been implemented by means of
7 analog electronic elements such as operational amplifiers, comparators and peak detectors, etc. [2]

8 The basic detection chain for a particle detector using analog electronics is shown in Fig. 1(a). The pulse
9 provided by the detector is integrated into the preamplifier to obtain a fast slope signal followed by a long
10 tail. This signal is typically filtered to obtain a quasi-Gaussian shaped output, a procedure usually known
11

*Corresponding Author

Email addresses: aregadio@srg.aut.uah.es (Alberto Regadío), ssanchez@srg.aut.uah.es (Sebastián Sánchez-Prieto),
mprieto@srg.aut.uah.es (Manuel Prieto), taberogj@inta.es (Jesús Tabero)

12 as pulse shaping, the purpose of which is to increase the Signal-to-Noise Ratio (SNR) in order to optimize
 13 detection [3]. In several detectors, the pulse charge is proportional to the energy of the detected particle.
 14 Also, the charge of the pulse is proportional to its amplitude. In these situations, a peak detector may be
 used to obtain a value proportional to the charge.

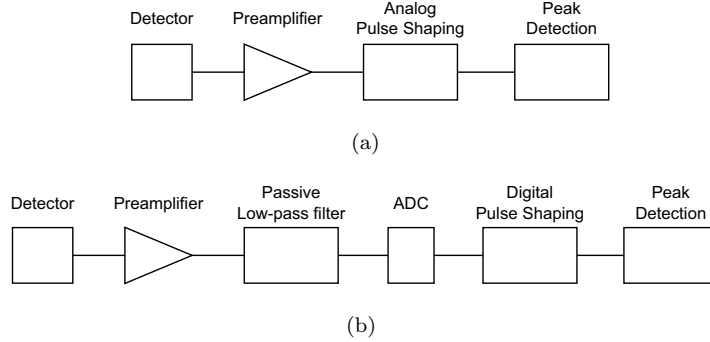


Figure 1: (a) Typical particle detection chain based on analog electronics. (b) Particle detector chain based on mixed analog-and-digital electronics.

15
 16 Nowadays, digital signal processing is also used in particle detectors [4, 5]. The proposed detection chain
 17 for a particle detector using digital signal processing is shown in Fig. 1(b). When the same detector and
 18 preamplifier from Fig. 1(a) are used, an Analog-to-Digital Converter (ADC) should be added after these
 19 stages to digitalize the signal. In addition, an optional analog filtering stage before the ADC could also be
 20 added. One objective of this study was to use this algorithm in a future satellite payload, an environment in
 21 which power requirements are very restrictive. Thus, one main objective was to reduce sampling frequency
 22 as much as possible in order to reduce power consumption. With this goal in mind, a passive low-pass
 23 filter was included between the preamplifier and the ADC. This was an anti-aliasing filter, which is typically
 24 used before an ADC, and its inclusion made it possible to fulfill the Nyquist criteria. The pole generates a
 25 low-pass filter that avoids the aliasing effect and thus, the sampling frequency could be decreased [6]. After
 26 the ADC, all processing, including shaping and peak detection, is performed using digital elements.

27 The ideal shaping for a detector depends on the input signal and the predominant noise [7]. Thus,
 28 specific techniques are used to synthesize various pulse shapers and optimize detection by maximizing the
 29 SNR [8, 9]. However, the noise spectrum can vary over time for several reasons (e.g. accumulated radiation on
 30 the detector, damage to the detector structure, etc. [1]), whereas these techniques do not usually consider
 31 noise variations in real-time [4, 5]. To avoid this drawback and allow the use of self-adjusting transfer
 32 functions, the use of adaptive shapers was proposed.

33 Several algorithms exist for performing adaptive shapers (e.g. Least-Mean-Square (LMS), Digital Pe-
 34 nalized LMS (DPLMS), Wiener algorithm and Discrete Fourier Transform (DFT) method [10, 11]). The
 35 LMS algorithm finds the filter coefficients associated with producing the least mean squares of the difference

36 between the desired and the actual signal. The DPLMS is an improvement on the LMS algorithm proposed
 37 in [10]. The Wiener algorithm minimizes the error by equating each partial derivative to zero. Finally, the
 38 DFT method is based on dividing the desired signal by a given input signal. The shape can also be adapted
 39 by modifying any of its parameters (e.g. the algorithm presented in [12] searches for the optimum shaping
 40 time).

41 In this paper, we propose a technique for automatic synthesis of digital pulse shapers for high-resolution
 42 spectroscopy using an adaptive algorithm based on the DFT and LMS methods. The proposed algorithm
 43 is suitable for real-time implementation and only requires simple hardware and an example pattern for
 44 training. The main advantage of this technique is that it has the capacity to transform any input signal
 45 into any output signal with the desired features (including typical shapes such as trapezoidal, triangular or
 46 cusp-like outputs).

47 In [10], algorithms for adaptive digital shaping with a good performance were presented; however, imple-
 48 mentation of most of these algorithms is quite complex. This complexity would also affect power consumption
 49 in a real implementation, which should be kept as low as possible. In addition, in the majority of these
 50 algorithms, the entire input signal must be known before calculating the filter coefficients, whereas the al-
 51 gorithm proposed here has the capacity to start adjusting the shaper coefficients as soon as the first pulse
 52 sample arrives. To sum up, the proposed design is a synthesizable algorithm that takes into account area,
 53 power consumption and above all, functionality.

54 **2. Proposed adaptive algorithm**

55 As explained in the Introduction, the utilization of different shaping techniques makes it possible to
 56 improve resolution in particle detectors [13]. Consequently, the aim of this study was threefold: to develop
 57 an automatic desired pulse shaping operation, to reduce input noise and to solve the pile-up effect. Of the
 58 design possibilities for obtaining the desired results, adaptive algorithms were selected because they have the
 59 capacity to automatically adjust the coefficients of a linear system and because they are easy to implement
 60 in digital hardware.

61 The proposed shaper works as an adaptive digital Finite Impulse Response (FIR) filter. The output of
 62 a FIR filter is given by the following expression:

$$y[n] = \sum_{k=0}^{N-1} a_k x[n-k] = h[n] * x[n] \quad (1)$$

63 where $x[n]$ is the input signal, $y[n]$ is the output signal, a_k are the coefficients of the filter, $h[n]$ its impulse
 64 response and N its order.

65 Two parameters related to digital filters are the shaping time τ_s , which is defined as the duration of the
 66 shaper output signal $y[n]$, and the ADC sampling period T_s . These are related to N as follows:

$$N = \frac{\tau_s}{T_s} \quad (2)$$

67 One method to adjust the a_k coefficients, which is described in [10], uses an iteration method to search
 68 for the solution that minimizes the error according to this formula:

$$h(z) = \frac{x(z)}{d(z)} \quad (3)$$

69 where $x(z)$ and $h(z)$ are the z-transform of $x[n]$ and $h[n]$, respectively, and $d(z)$ is the z-transform of the
 70 desired output signal $d[z]$. This is one of the simplest methods for adapting a shaper. Thus, implementing
 71 it in an FPGA yields a low occupation area and low power consumption, one of the objectives of this study.
 72 However, several drawbacks of this method are described in [10], including output signal undershoots and
 73 the possibility that the filter order is infinite (i.e. it does not belong to the FIR class). To minimize the
 74 effects of these drawbacks and obtain better results, the lengths of $x[n]$ and $d[n]$ should be equal or the
 75 length of $d[n]$ should be slightly smaller than the length of $x[n]$. This is because when $x[n]$ is equal to zero
 76 during several cycles at the end of the pulse, the shaper needs a_k coefficients with high values to obtain
 77 $d[n]$ at the output. Therefore, the coefficients at the end are much greater than those at the beginning,
 78 producing an increase in the undershoot and a poor adaptation depending on $x[n]$.

79 One method to mitigate noise and phase shift is to replace $x[n]$ by the mean value of Λ input signals;
 80 however, this does not work properly unless the input pulses have the same shape and duration. Furthermore,
 81 the sampling frequency should be sufficiently high to ensure a negligible phase shift between pulses. Thus,
 82 there are many applications in spectroscopy where this procedure cannot be applied, and Λ shall be equal
 83 to one.

84 3. Design

85 As indicated in the Introduction, the proposed design was conceived with two goals in mind: simplicity
 86 and low power consumption. Therefore, it was important to reduce the functional units and working
 87 frequency as much as possible. Furthermore, both the shaper and peak detector were implemented in the
 88 same FPGA.

89 In this design, the output pulse $y[n]$ is converted into a desired pulse $d[n]$ by adjusting the shaper
 90 coefficients in real-time as a function of an input signal $x[n]$.

91 Both $x[n]$ and $d[n]$ are introduced into the shaper at the same time. According to (2), both N and T_s
 92 must be set manually before the shaper adjusts its coefficients. The correct T_s depends on the duration of
 93 the input pulses.

94 In order to synchronize $x[n]$ and $d[n]$, this last signal is provided when $x[n]$ is greater than a predefined
 95 learning threshold, which should be equal to or greater than the pulse-height analysis threshold. Thus, the

96 shaper only “learns” when a desired input pulse arrives, avoiding possible false triggers due to noise and
 97 undesired pulses.

98 Fig. 2 shows a detailed diagram of the shaper. The *den* signal is used to enable the learning process.
 99 The error $e[n]$ is obtained by subtracting the reference signal $d[n]$ from the output signal $y[n]$ and is used
 100 to adjust the coefficients signaled by the Register Selector which enables one register each clock cycle while
 101 the *den* signal remains at high-level. The structure inside the box must be repeated N times, where N is
 102 the order of the shaper. For each sample from the input signal, a coefficient a_i is adjusted. The process
 103 ends when all the filter coefficients have been adjusted. In this moment, the *den* is disabled and the overall
 104 shaper works as a filter. If so desired, the learning process can repeated by once again enabling the *den*
 105 signal.

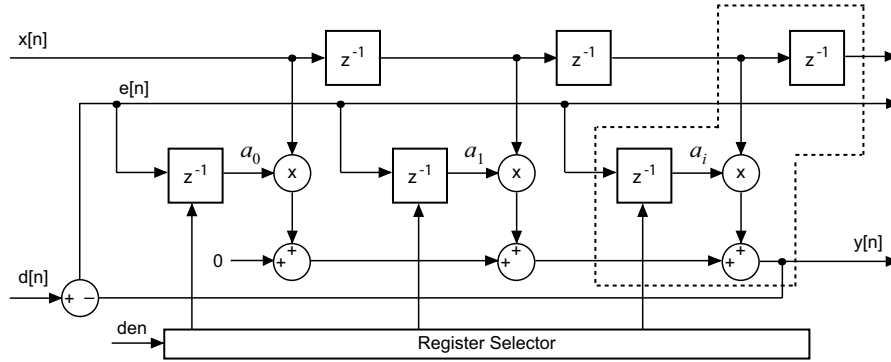


Figure 2: Block diagram of the third order adaptive shaper using one learning cycle.

106 4. Implementation

107 The overall design was implemented in VHDL. The order of the shaper N and the input/output signal
 108 width W are configurable parameters. The structure proposed in Fig. 2 can be translated into VHDL code
 109 for implementation in the FPGA using the following pseudocode:

```

 $a(1..N) \leftarrow 0;$ 
for  $i = 1$  to  $N$  —learning process
   $x(1) \leftarrow x;$ 
  for  $j = 2$  to  $N$  —shift register
     $x(j) \leftarrow x(j - 1);$ 
  end for;
  if  $i = 1$  then
     $a(1) \leftarrow d(1)/FP;$ 
  else

```

```

 $y \leftarrow \sum_{j=1}^N x(j) \cdot a(j);$ 
 $e \leftarrow d(i) - y(i);$ 
 $a(i) \leftarrow e/FP;$ 

```

```

end if;

```

```

end for;

```

110 where FP is the fixed-point parameter used to adjust the scale of the values used. The lower the value
 111 of this parameter, the better the adaptive shaper fits to the desired signal; however, a low value of FP could
 112 cause an overflow. Therefore, the FP should be adjusted specifically for each detection chain. It is strongly
 113 recommended that this value is a power of two to simplify the division operation.

114 In accordance with Fig. 2 and the pseudocode presented, for each order of the shaper, an adder, a
 115 multiplier and two flip-flops, all of them with width W are synthesized. In this way, the resources used for
 116 a given device can be estimated. As explained in Section 3, both shaper and detector are synthesized in the
 117 same digital chip.

118 5. Test results

119 Two types of test were performed: simulation tests and real experimental tests using a NIM module. In
 120 both cases, it was assumed that when a particle is detected, the preamplifier stage will generate the following
 121 pulse:

$$x(t) = A \exp\left(\frac{-t}{\tau_1}\right) \quad (4)$$

122 where A is the pulse amplitude and τ_1 the adjustable constant decay. As stated in Section 1, in traditional
 123 spectroscopy systems, an analog shaper that produces a semi-Gaussian pulse usually follows the detector-
 124 preamplifier configuration. As described in the Introduction, in order to reduce T_s , the preamplifier is
 125 followed by a low-pass RC filter as an analog shaper. Thus, when it is fed with the pulses (4), the CR-RC
 126 output becomes:

$$x(t) = A \frac{\tau_1}{\tau_1 - \tau_2} \left(\exp\left(\frac{-t}{\tau_1}\right) - \exp\left(\frac{-t}{\tau_2}\right) \right) \quad (5)$$

127 Pulses similar to the one described in Eq. (5) were processed with the adaptive shaping presented in
 128 this paper. Finally, at the end of the chain, a peak-detector captured the maximum values of the signals
 129 generated by the digital shaper, and these values were used to measure chain detection performance.

130 5.1. Simulation tests

131 These tests consisted of simulating the adaptive shaper in a digital design tool, using the Mentor Graphics
 132 ModelSim SE 6.2c software package using CR and CR-RC as input signals. Although CR-RC shaping is
 133 usually carried out using $\tau_1 = \tau_2$ [1], we selected $\tau_1 = 100 \mu\text{s}$ and $\tau_2 = 1 \mu\text{s}$ as the time constants in order

134 to obtain signals with a similar shape (but with different shaping time τ_s) to the signals coming from the
 135 facility described in Section 6. The input/output signals were processed with 14-bit resolution at 2.5 MHz
 136 because this is the resolution of the ADC used in the experimental test.

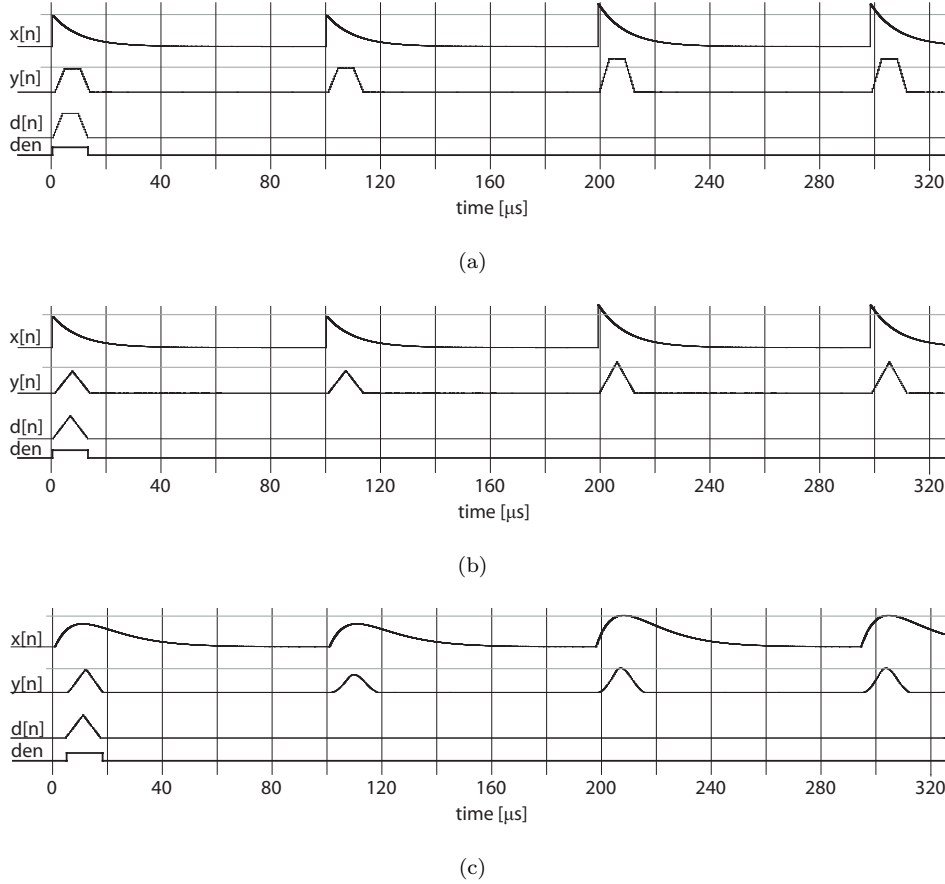


Figure 3: Simulation of the learning process (first pulse) and shaping for 32-order trapezoidal (a), and triangular (b, c) shapers.

137 Although the proposed shaper has the capacity to synthesize a wide range of output signals, in this study
 138 the simulation tests were performed using trapezoidal and cusp-like shaping because these shapers are used
 139 extensively [5, 9]. In addition, triangular shaping was also used in this test because this is the optimum
 140 type for white noise [7]. To simplify the tests, the rising and falling edge of the trapezoidal shaper was $N/4$
 141 cycles long and the flat-top was $N/2$ cycles long in all tests (simulation and experimental) for a given order
 142 filter N . In triangular and cusp-like shaping, the edges were also symmetrical.

143 The duration of the CR input pulse (Fig. 3(a) and 3(b)) is just over $12 \mu\text{s}$. This time is similar to the
 144 duration of the signals used in this section. According to Eq. (2), if this example was carried out using
 145 shapers with $N = 32$, the sampling frequency $f_s = 1/T_s$ should be approximately 2.5 MHz. Note that
 146 when the duration of a pulse is low with respect to the duration of the pulse used to adjust the coefficients
 147 (fast pulses), the pulse will not be captured correctly unless the sampling frequency changes and the shaper

148 adjusts its coefficients again. Although this seems a low clock frequency for an actual digital system, on the
 149 one hand the ultimate objective was to use this algorithm in a satellite payload where power requirements
 150 are very restrictive, and thus the sampling frequency should be reduced as much as possible, and on the
 151 other hand, according to [6], if a Gaussian signal is sampled at 2.5 MHz, the energy variation estimation is
 152 negligible compared to another noise sources.

153 Fig. 3 shows the output of the proposed 32-order shaper working at a $f_s = 2.5$ MHz for a CR input (Figs.
 154 3(a), 3(b)) and a CR–RC input (Fig. 3(c)). In all the figures, the first and second $x[n]$ pulses are smaller
 155 than the third and fourth to show the effect of scaling on $y[n]$. The signals $d[n]$ and den are the desired
 156 signal and the learning enable, respectively. Thus, the learning process is active when den is active-high. It
 157 can be observed in Fig. 3(c) that the pulses are worse shaped than those shown in Figs. 3(a) and 3(b). This
 158 is because when $x[n]$ has a high maximum, a_k coefficients are also adjusted with high values, minimizing
 159 the effect of rounding to the nearest integer. Minimizing this effect implies a greater similarity between $y[n]$
 160 and $d[n]$.

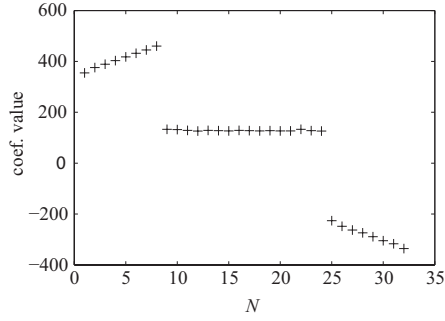
161 After each learning iteration using the input/output signal in Fig. 3(a), the coefficients were automati-
 162 cally adjusted as shown in Fig. 5.1. As can be seen, the coefficients of the shaper were very similar to the
 163 static coefficients of the trapezoidal shaper presented in [14], leading us to confirm that the shaper had been
 164 synthesized correctly.

165 The effect on shaping when the input signal varies in duration is similar to the effect produced using non-
 166 adaptive shapers since equal shapers produce equal results independently of the method applied to calculate
 167 their coefficients. Fig. 5 shows the effect on an adaptive trapezoidal shaping when the time constant τ_1 of
 168 the CR pulse varied. The shaper used was the same as the one whose coefficients are depicted in Fig. 4(a).
 169 It produced a trapezoid when the input signal was a CR pulse of $\tau_1 = 1 \mu s$. As can be seen, these variations
 170 affected pulse height and consequently, resolution. Therefore, time variations should be minimized.

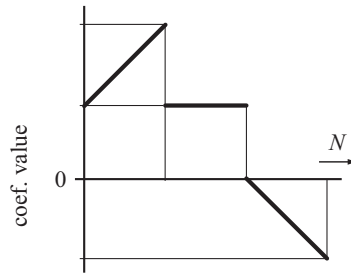
171 Independently of the coefficients obtained, the shaper is linear and time-invariant; thus, it can facilitate
 172 the detection of pile-up events. Fig. 6 shows a pile-up event, in which the first signal has twice the amplitude
 173 of the second one. For pile-up management, a pile-up event processing stage should be included between
 174 the digital shaper and the peak detector [15].

175 5.2. Experimental results using a reference pulser

176 After the shaper had been successfully simulated, it was tested using a real benchmark. In this scenario,
 177 the pulses explained at the beginning of this section were generated using a Canberra Model 1407 Reference
 178 Pulser of a Nuclear Instrumentation Module (NIM). This NIM generates a group of periodic pulses of equal
 179 amplitude that can be fed into the test input of the preamplifiers or the shapers. It generates an exponential
 180 pulse identical to those produced by the detector-preamplifier, which can be fed in at the ADC stage (see
 181 Fig. 1(b)).



(a)



(b)

Figure 4: Coefficients of an automatically synthesized a_k trapezoidal shaper ($N = 32$) (a) vs. a trapezoidal shaper impulse response (adapted from [14]) (b). In both cases, the input signal is a CR pulse.

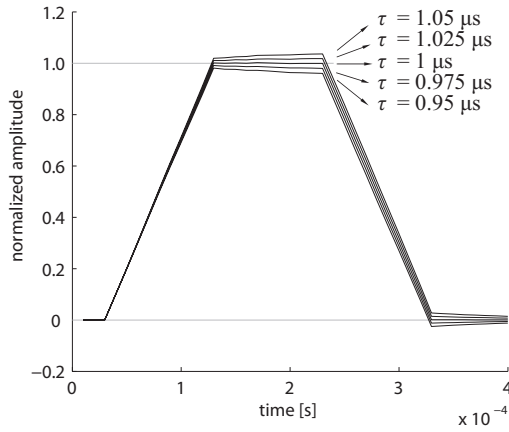


Figure 5: Effect on shaping when the input signal varies in time duration. This shaper is adjusted to obtain a trapezoidal shape when the input signal is a CR pulse with $\tau_1 = 1 \mu\text{s}$.

182 The reference pulse generator was adjusted to obtain a time constant $\tau_1 = 100 \mu\text{s}$ and $\tau_2 = 1 \mu\text{s}$. No
 183 more analog electronics were required after the analog shaper, except for the ADC (see Fig. 1), a Texas
 184 Instruments 14-bit (ADS5474) with up to 25 MS/s. With these values, Eq. (2) can be used to obtain the
 185 sampling frequency for a given shaper order N (Table 1). Following the ADC, an FPGA was used to perform

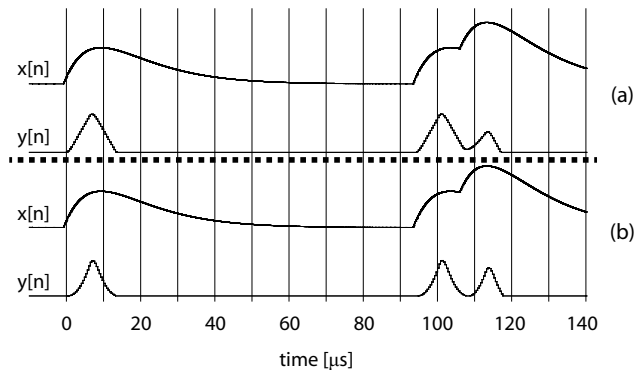


Figure 6: Simulation of the pile-up effect for a triangular (top), and cusp-like (bottom) using trained 32-order shapers.

186 the rest of the processing (pulse shaping and pulse-height analysis). Besides, to adjust f_s , the FPGA drives
 187 the ADC input clock. FPGA logic were implemented in a Xilinx Virtex-4 FPGA (XC4VFX60-11FF1152).
 188 Finally, a Xilinx ChipScope Pro 10.1 was employed to capture the pulse amplitudes using the JTAG port.

Table 1: Shaper order N and the corresponding sampling frequencies f_s used in the experimental tests. M is the flat-top number of samples of the trapezium and $L = \frac{N-M}{2}$ its number of edge samples.

N	L	M	f_s
16	4	8	625 kHz
32	8	16	1250 kHz
40	10	20	1562.5 kHz
56	14	28	2187.5 kHz
64	16	32	2500 kHz
80	20	40	3125 kHz

189 Once the input signal and the shaping type have been selected, the shaper learns with the method
 190 explained in Section 3. To test how the shaper worked, a trapezium was synthesized. The results for each
 191 of the shapers shown in Table 1 are given in Fig. 7, where it can be seen that the trapezoidal shape was
 192 obtained from $N = 32$.

193 One key parameter to measure the quality in spectroscopy of the energy resolution is the Full Width at
 194 Half Maximum (FWHM). Thus, the proposed shaper can be characterized by determining the FWHM of a
 195 group of identical signals produced with a precision pulse generator. The FWHM results for one pulse and
 196 the mean of five pulses ($\Lambda = 1$ and $\Lambda = 5$, respectively) are shown in Fig. 8. For this statistical analysis,
 197 10000 pulses of equal height were used throughout the test. The FWHM values were calculated from the
 198 pulse height histograms. These calculations were performed using Matlab, and the histograms were not
 199 fitted with any kind of function.

200 Although the energy error of the generated pulse should ideally be zero, it can be seen that the FWHM
 201 was inversely proportional to the order of the shaper. Thus, the FWHM increased because of a phase shift
 202 between pulses due to the sampling frequency. For this reason, the gap between the shapers trained with
 203 $\Lambda = 1$ and $\Lambda = 5$ became smaller when N was increased. Therefore, for a high N , adjusting the shaper with
 204 just one pulse may be sufficient.

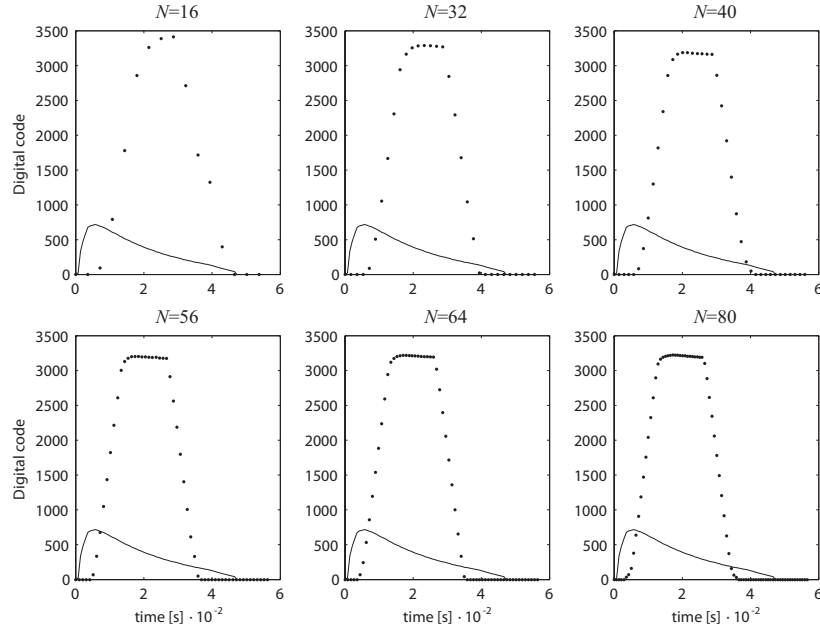


Figure 7: Input signal (solid line) and its corresponding trapezoidal shape (dotted line) for different orders of the shaper N using one learning iteration.

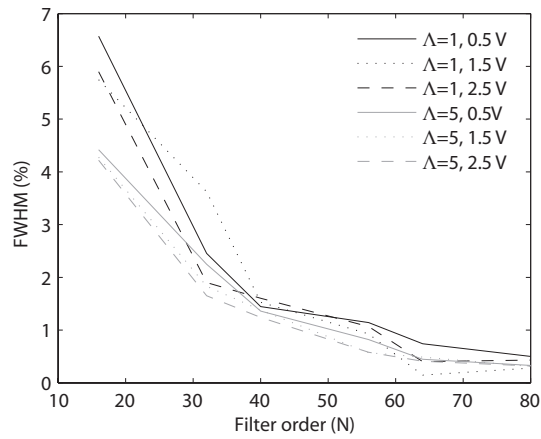


Figure 8: Results of FWHM with $\Lambda = 1$ and $\Lambda = 5$ for different shaper orders and amplitude levels of the signal that arrives at the digital shaper after the ADC stage.

205 As stated at the beginning of this section, both shaping and peak detection stages were synthesized in

206 the same FPGA using a Xilinx ISE 13.1 developing tool. Table 2 shows the resources used and the power
 207 consumption, measured using current probes. As can be seen, power consumption rose slowly as the order
 208 of the shaper increased.

Table 2: Comparison of FPGA (Xilinx XC4VFX60-11FF1152) performance and power consumption when implemented with different N .

N	DSP48 (%)	Slices (%)	FPGA power consumption
16	8 (6%)	622 (2%)	265 mW
32	16 (12%)	1013 (4%)	275 mW
40	20 (15%)	1209 (5%)	280 mW
56	28 (21%)	1519 (6%)	285 mW
64	32 (25%)	1811 (7%)	295 mW
80	40 (31%)	2220 (8%)	310 mW

209 6. Experimental results using a neutron monitor

210 Lastly, a test to check the proposed shaper was performed. The main objective of this test was to
 211 obtain similar results to those obtained in experiments carried out with a non-adaptive shaper. This test
 212 was performed in the Castilla-La Mancha Neutron Monitor (CaLMa) located in Guadalajara, Spain. The
 213 instrument consisted of fifteen proportional gas counter tubes. More information about features, setup and
 214 results of this instrument can be found in [16]. In both the cited experiment and the present test, an
 215 LND2061 tube connected to a Canberra ACHNA98 amplifier followed by an AmpTek 8000A Multichannel
 216 Analyzer were used. A complete setup of the experiment is shown in Figs. 9 and 10. The Data Acquisition
 217 Board (DAQ) was a proprietary design, whereas the Digital Processing Board was an evaluation board
 218 (Xilinx ML410).

219 In real particle detectors, the pulses can have a different duration and amplitude. This is the case of
 220 the detector at this facility. When this occurs, the user must define a region of interest based on previous
 221 experiences (according to Fig. 12(a), between channels #260 and #300). If it is not possible to define
 222 a region of interest, the adaptive shaper simply operates as an adaptive FIR filter. However, the main
 223 objective of a shaper is not to obtain an output signal with a “perfect” shape, but to obtain the maximum
 224 SNR.

225 To perform the test using the adaptive shaper, the preamplifier was connected to a proprietary data
 226 acquisition system with an ADC core. This device was a 14-bit Linear LTC2171 working at a dynamically
 227 selectable frequency of up to 40 MS/s. Following the ADC, a ML410 board, whose core was the digital

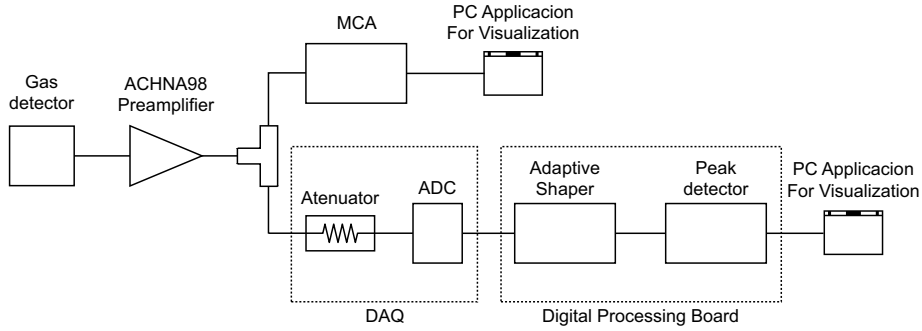


Figure 9: Setup of the neutron monitor experiment.

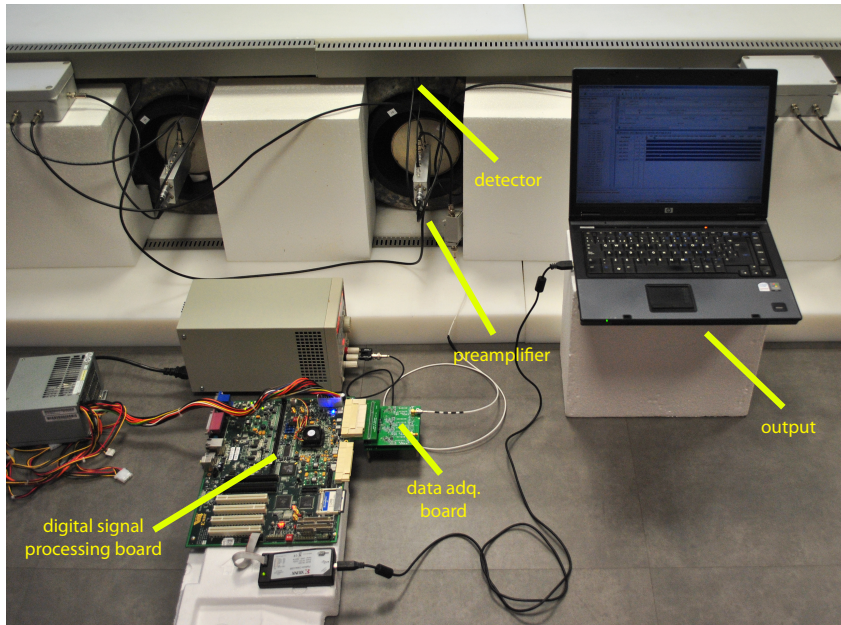


Figure 10: Image of the setup of the neutron monitor for this experiment.

228 system explained in Section 5.2, included the described adaptive shaper and the peak detector. Both boards
 229 transmitted and received data through LVDS signals. We selected the beginning of the region of interest
 230 (channel #260) as the learning threshold of the shaper.

231 An optimal shaper depends on the facility's noise type. Thus, it should be calculated by means of a
 232 procedure (e.g. [3] or [7]) to enable the adaptive shaper to transform the input signal into the optimal shape.

233 Using a spectrum analyzer, it was observed that the predominant noise was white noise. Therefore, in
 234 accordance with [7], a triangular shaping for the region of interest with $N = 32$ and $f_s = 1/T_s = 10$ MS/s
 235 was used for this setup. The histogram obtained is shown in Fig. 12(b) whereas the histogram obtained with
 236 the Multichannel Analyzer is shown in Fig. 12(a). Both histograms were created using the 65000 samples
 237 with the highest amplitude from a set of 90500. The measured energy spectrum was 2.31 MeV (channel

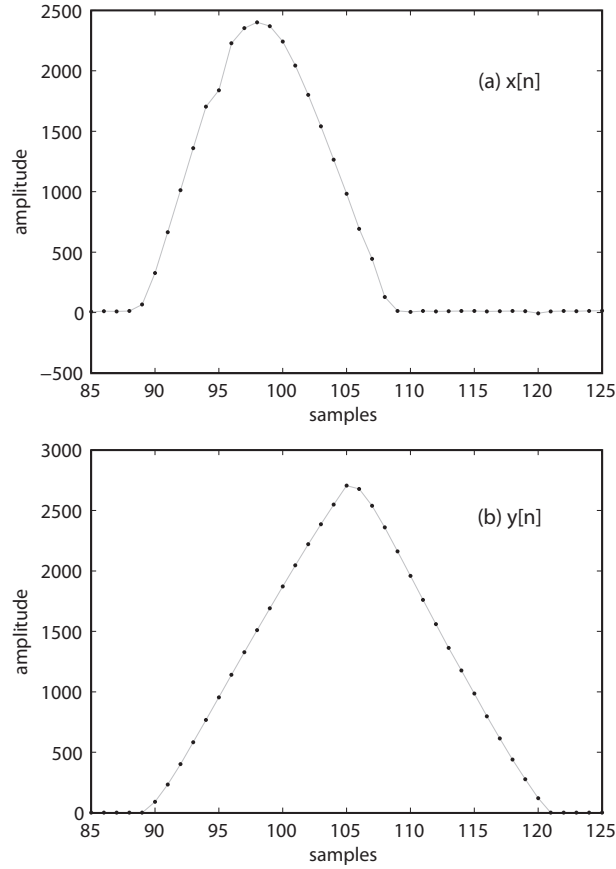


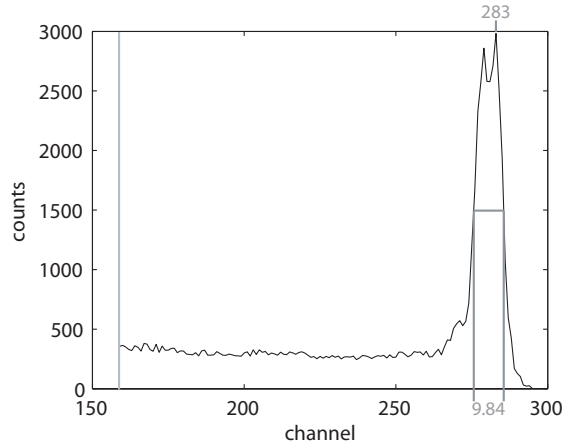
Figure 11: Results obtained with the adaptive shaper inside the FPGA using a pulse coming from the preamplifier. The signal was sampled at 10 MHz. (a) Pulse event; (b) Corresponding triangular shape.

238 #300), and the duration of the test was 8 hours. Thus, the average event rate was 3.1 per second.

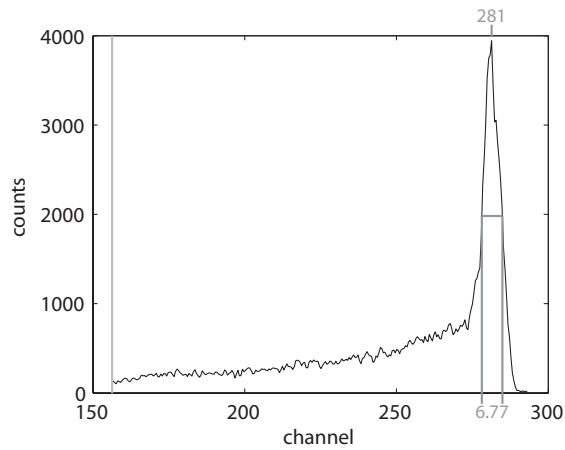
239 In the case of using the adaptive shaper, a FWHM equal to 6.77 (2.41%) was obtained, whereas in the
 240 case of the histogram created with the MCA, a FWHM equal to 9.84 (3.48%) was obtained. It is important
 241 to consider that the MCA does not apply any shaping, whereas in this test, the triangular shaping of Fig.
 242 11(b) was applied to reduce the white noise. However, a comparison of both figures indicates the similarity of
 243 the FWHM of the histograms from both experiments. It may be reasonable to assume that the differences in
 244 the histograms were the result of using different detection chains to generate them (see Fig. 9). In fact, the
 245 histogram of Fig. 12(a) was generated using an analog MCA with no previous digital shaping whereas the
 246 histogram of Fig. 12(b) was generated using an ADC, digital adaptive shaping and digital peak detection.

247 7. Conclusions

248 In this study, a new adaptive digital shaper for real-time spectroscopy was designed and implemented in
 249 an FPGA. This proposed adaptive shaper is an effective means of generating a desired shape by automatically



(a)



(b)

Figure 12: Histogram for pulses obtained using (a) the AmpTek 8000A Multichannel Analyzer and (b) the proposed adaptive shaper. The grey lines indicate the threshold level.

250 adjusting the coefficients of the shaper using the input signal during a learning period. A high sampling
 251 rate increases power consumption, but a low sampling rate could deteriorate the FWHM; therefore, a good
 252 reference point must involve a trade-off between these parameters. The most common pulse shape methods
 253 were successfully tested in simulations. As regards the type of noise present in a real benchmark, the optimal
 254 shaper for this noise was tested. As with the other non-adaptive shapers, the FWHM of the histograms
 255 was reduced when the shaper order was increased, due to sampling effects. Lastly, we have shown that the
 256 increase in resolution when shapers are trained using five signals instead of one is negligible for high order
 257 shapers. The proposed shaping method allows for the generation of histograms with a resolution comparable
 258 to classical analog shaping alternatives. Thus, this represents a promising method, regardless of whether
 259 power consumption or simplicity is the main consideration.

260 Acknowledgments

261 This project was funded by the Spanish Administration as part of project ref. AYA2012-39810-C02-02.
262 The authors thank the CaLMa Team for technical support and for providing the CaLMa facility.

263 Bibliography

- 264 [1] G. F. Knoll, *Radiation Detection and Measurement*. John Wiley & Sons, Inc. 2000.
- 265 [2] P. W. Nicholson, *Nuclear Electronics*. John Wiley & Sons, Ltd., 1973.
- 266 [3] E. Gatti, A. Geraci, G. Ripamonti, “Automatic synthesis of optimum filters with arbitrary constraints and noises: a new
267 method”. *Nuclear Instruments and Methods in Physics Research A* 381 (1996) 117–127.
- 268 [4] D. Alberto et al., “FPGA implementation of digital filter for nuclear detectors”. *Nuclear Instruments and Methods in
269 Physics Research A* 611 (2009) 99–104.
- 270 [5] A. M. Fernandes, et al. “Parallel processing method for high-speed real time digital pulse processing for gamma-ray
271 spectroscopy”. *Fusion Engineering and Design* 85 (2010) 308–312.
- 272 [6] R. Abbiati, A. Geraci, G. Ripamonti, “Analog Shaping Optimization for Digital Processing of Radiation Detector Signals”.
273 *IEEE Transactions on Nuclear Science*, vol. 52, no. 5, October 2005.
- 274 [7] F. S. Goulding, “Pulse-Shaping in Low-Noise Nuclear Amplifiers: A Physical Approach to Noise Analysis”. *Nuclear
275 Instruments and Methods* 100 (1972) p.493–504.
- 276 [8] M. Nakhostin, “Recursive Algorithms for Real-Time Digital CR–(RC)ⁿ Pulse Shaping”. *IEEE Transactions on Nuclear
277 Science*, vol. 58, no. 5, October 2011.
- 278 [9] V. T. Jordanov, “Exponential Signal Synthesis in Digital Pulse Processing” *Nuclear Instruments and Methods in Physics
279 Research A*, 670 (2012) 18–24.
- 280 [10] E. Gatti, A. Geraci, S. Riboldi, G. Ripamonti. “Digital Penalized LMS method for filter synthesis with arbitrary constraints
281 and noise”. *Nuclear Instruments and Methods in Physics Research A* 523 (2004) 167–185.
- 282 [11] A. V. Oppenheim, R. W. Shafer, *Discrete-Time Digital Signal Processing*. 3rd Ed. Pearson Education, 2010.
- 283 [12] A. Abba, A. Geraci, “Dynamic Maximization of Filter Length in Digital Spectroscopy”. *IEEE Transactions on Nuclear
284 Science*, vol. 59, no. 5, october 2012.
- 285 [13] J. Beringer et al. (Particle Data Group), *Physical Review D* 86, 010001 (2012). [<http://dx.doi.org/10.1063/1.1898643>]
- 286 [14] V. T. Jordanov, G. F. Knoll, “Digital synthesis of pulse shapes in real time for high resolution radiation spectroscopy”.
287 *Nuclear Instruments and Methods in Physics Research A* 345 (1994) 337–345.
- 288 [15] C. Imperiale, A. Imperiale. “On nuclear spectrometry pulses digital shaping and processing”. *Measurement* 30 (2001)
289 49–73.
- 290 [16] J. Medina, et al., *Nuclear Instruments and Methods in Physics Research A* (2013),
291 <http://dx.doi.org/10.1016/j.nima.2013.06.028i>